HHS Public Access

Author manuscript

J Bone Miner Res. Author manuscript; available in PMC 2016 March 07.

Published in final edited form as:

J Bone Miner Res. 2015 September ; 30(9): 1608–1617. doi:10.1002/jbmr.2494.

Mesenchymal Deletion of Histone Demethylase NO66 in Mice Promotes Bone Formation

Qin Chen[*], **Krishna Sinha**[1], **Jian Min Deng**, **Hideyo Yasuda**[2], **Ralf Krahe**, **Richard R. Behringer**, and **Benoit de Crombrugghe**[#]

Department of Genetics, The University of Texas MD Anderson Cancer Center, 1515 Holcombe Blvd., Houston, TX 77030, USA

Abstract

Our previous studies indicated that the Jumonji C (JmjC)-domain-containing NO66 is a histone demethylase with specificity for methylated histone H3K4 and H3K36. NO66 binds to the transcription factor Osterix (Osx) and inhibits its transcriptional activity in promoter assays. However, the physiological role of NO66 in formation of mammalian bones is unknown. Here, using a genetically engineered mouse model, we show that during early skeletal development, *Prx1-Cre* dependent mesenchymal deletion of *NO66* promotes osteogenesis and formation of both endochondral as well as intramembranous skeletal elements, leading to a larger skeleton and a high bone mass phenotype in adult mice. The excess bone formation in mice where *NO66* was deleted in cells of mesenchymal origin is associated with an increase in the number of preosteoblasts and osteoblasts. Further analysis revealed that in the embryonic limbs and adult calvaria of mice with deletion of *NO66* in cells of mesenchymal origin, expression of several genes including *bone morphogenetic protein 2, insulin-like growth factor 1* and osteoclast inhibitor *osteoprotegerin* was increased, concurrent with an increase in expression of bone formation markers such as *Osx*, *type I collagen* and *bone sialoprotein*. Taken together, our results provide the first *in vivo* evidence that NO66 histone demethylase plays an important role in mammalian osteogenesis during early development as well as in adult bone homeostasis. We postulate that NO66 regulates bone formation, at least in part, via regulating the number of bone-forming cells and expression of multiple genes that are critical for these processes.

Introduction

Mammalian bone is formed via two different mechanisms--intramembranous and endochondral ossification. Both mechanisms involve commitment of mesenchymal precursors that differentiate into osteochondroprogenitors, from which osteoprogenitors or preosteoblasts segregate and then further differentiate into mature osteoblasts and later in

[*]Correspondence: Qin Chen, M.D., Department of Genetics, The University of Texas MD Anderson Cancer Center, 1515 Holcombe Blvd., Houston, TX 77030. qchen1@mdanderson.org; Phone: +1 713-834-6346; Fax: +1 713 792 1470. [#]Co-correspondence: Benoit de Crombrugghe, M.D., Department of Genetics, The University of Texas MD Anderson Cancer Center, 1515 Holcombe Blvd., Houston, TX 77030. bdecromb@mdanderson.org; +1 713-834-6376; Fax: +1 713 834 6396.

[1]Current address: Department of Endocrine Neoplasia and Hormonal Disorders, The University of Texas MD Anderson Cancer Center, 1515 Holcombe Blvd., Houston, TX 77030, USA

[2]Current address: Department of Animal Biotechnology, College of Animal Biosciences and Technology, Konkuk University, Seoul 143-701, Korea

osteocytes to form bone tissue. This process integrates expression of diverse signaling molecules including *bone morphogenetic protein 2 (Bmp2)* and *insulin-like growth factor 1*(*Igf1*), as well as key transcription factors such as *runt-related transcription factor 2 (Runx2), osterix* (*Osx*), and *β-catenin*. [1-6] Expression of *Runx2* is known to begin in the notochord on mouse embryonic day 9.5 (E9.5); it is later restricted to prechondrogenic mesenchymal condensation and chondrocytes and then in osteoblast lineage cells. [3, 6] *Osx* expression first appears in the perichondrium/periosteum in mouse embryos on E13, and is essential to formation of osteoblast lineage cells. [4-6] In *Runx2* deficient mice (*Runx2*$^{-/-}$), no osteoblast differentiation occurs and no endochondral and intramembranous skeletal elements form beyond the stage of cartilage anlagens. [1-3] Similarly, in *Osx*$^{-/-}$ mice, formation of both endochondral and intramembranous bones was completely abolished. [4] Expression of *Runx2* and *Osx* is regulated by a broad signaling network including members of BMP, IGF and Wnt families. [7-11]

In recent years, histone methylation has been shown to be of great importance in the control of gene expression. Methylation of H3K4 and H3K36 is associated with gene activation. [12, 13] It has been demonstrated that histone methylation can be eliminated by demethylases. [14, 15] Members of the Jumonji C (JmjC)-domain-containing protein family encode a large class of histone demethylases. NO66 is a member of the JmjC-domain-only subfamily. [14] It was previously described as a component of nucleoli in oocytes of *Xenopus laevis*. [16] The physiological role of NO66 remains largely unexplored, however. NO66 was shown to be associated with c-Myc, [17] was also observed to function as a stress-responsive mediator in *Caenorhabditis elegans*, [18] and was identified in human optic nerve head lamina cribrosa cells in response to mechanical strain. [19] We previously demonstrated that NO66 harbors histone demethylase activity that is specific for methylated H3K4 as well as H3K36, and that NO66 binds to Osx and inhibits its activity in reporter assays. [20] We also showed that knockdown of *NO66* in MC3T3 preosteoblasts increases expression of Osx-downstream targets, *bone sialoprotein (Bsp)* and *Osteocalcin (Oc)*. Moreover, during the induced differentiation of MC3T3 preosteoblasts, NO66 occupancy in the chromatin of *Bsp* and *Oc* genes decreases, whereas levels of trimethylated histone H3 at lysine 4 (H3K4me3) and lysine 36 (H3K36me3) in the chromatin of those genes increase.[20] It was reported that NO66 can be recruited to the Polycomb Repressive Complex 2 (PRC2) during embryonic stem cell differentiation, leading to loss of H3K36me3 and transcriptional silencing of previously active genes, [21] highlighting an important role for NO66 in gene regulation.

To study the physiological role of NO66 in mammalian osteogenesis, we generated conditional knockout mice in which *NO66* was inactivated in cells of *Prx1-Cre* expressing mesenchymal lineage. We found that mesenchymal deletion of *NO66* accelerated bone development in embryos, leading to high bone mass in mice at adult stages.

Materials and Methods

Generation and Genotyping of *NO66flox* and *Prx1-Cre; NO66*$^{f/f}$ Mice

A 12-kb fragment containing the *NO66* promoter and coding region was retrieved from a BAC (BACPAC Resources Center) and inserted in the pBluescript SK vector via recombineering approach. Using bacterial recombination, a *PGK-neo* cassette flanked by

FRTs and two *LoxP* sites were introduced into the pBluescript SK vector to generate a *NO66*-targeting vector (Fig. 1A), which was then electroporated into G4 (C57BL/6Ncr × 129S6) mouse embryonic stem (mES) cells. Integration of the targeting vector into the *NO66* locus was confirmed via Southern blot hybridization (Fig. 1C) and polymerase chain reaction (PCR) (Fig. 1D). Two positive mES clones were randomly selected and microinjected into C57BL/6J blastocysts to generate *NO66flox* mice, which were then crossed with *Prx1-Cre* mice [22] to generate *Prx1-Cre; NO66*$^{f/+}$ and *Prx1-Cre; NO66*$^{f/f}$ mice. Genotyping of mice see Supplemental Material & Methods.

RNA Isolation and Quantitative Real-Time PCR (qPCR)

Total RNA of different murine tissues were isolated using TRIzol reagent (Invitrogen; 15596-018) according to the manufacturer's protocol. QPCRs see Supplemental Material & Methods.

Histology

For histological analyses, paraformaldehyde-fixed, paraffin-embedded embryonic undecalcified or adult decalcified mouse tissue sections were stained with Alcian blue, Safranin O, and hematoxylin & eosin following routine experimental procedures. To examine mineral deposition in bones, long bone and calvarial tissue sections were stained using von Kossa's experimental approach and then counterstained with Nuclear Fast Red as described previously. [4, 5]

Immunofluorescence and Western Blots

For detection of bone matrix proteins, paraffin-slides were deparaffinized and subjected to epitope retrieval using enzymatic digestion with hyaluronidase (2 mg/mL in phosphate buffer, pH 5.5; MP Biomedicals). For detection of Osx, NO66, H3K4me3 and H3K36me3, tissue slides were boiled in 10 mM sodium citrate buffer (pH 6.0) for 15 min using a microwave oven to expose antigen. Primary and secondary antibodies see Supplemental Material & Methods. For Western blots, nuclear lysates of femurs from embryos at embryonic day 18.5 (E18.5) were isolated using NE-PER Nuclear and Cytoplasmic Extraction kit (Pierce, Rockford, IL) following manufactory instruction. Antibodies against H3K4me3, H3K36me3 and histone H3 were obtained from Abcam (Cambridge, MA). The Western blots were performed following experimental procedure described previously. [23, 24]

BrdU and Calcein Incorporation

For cell proliferation assay, 5-bromo-2′-deoxyuridine (BrdU) (100 μL/10g body weight; Invitrogen) was injected into pregnant female mice. Two hours later, the mice were sacrificed and analyzed using immunofluorescence staining as described previously. [24] For Calcein labeling, mice were given twice intraperitoneal injection with calcein solution (10 mg/ml, diluted in 2% $NaHCO_3$, PH 7.4; 10 mg calcein per kg body weight). The second injection was performed five days after the first injection, and two days before the injected mice were sacrificed.

μCT and Histomorphometry

Femurs and calvaria of adult male mice were fixed in 4% paraformaldehyde overnight and stored in 70% ethanol for μCT scanning (eXplore GE Locus SP; GE Healthcare). The resulting images were analyzed using the MicroView software program (version 2.2; GE Healthcare). Histomorphometry was performed using an OsteoMeasure histomorphometry system (OsteoMetrics) (see Supplemental Material & Methods).

Statistical Analysis

All statistical results are presented as the mean ± standard deviation (S.D.). The differences between groups were calculated using the two-tailed Student *t*-test. P values less than 0.05 were considered statistically significant.

Results

Generation of *NO66flox* and Mesenchyme-Specific *NO66*-Knockout Mice

Since NO66 is widely expressed, [19] we first generated *NO66flox* mice, in which the single exon of *NO66* is flanked by two *LoxP* sites (Fig. 1A). To delete the *NO66* gene in cells of mesenchymal lineage, we generated *Prx1-Cre; NO66flox/flox* (*Prx1-Cre; NO66*$^{f/f}$) mice, where expression of Cre was driven by the *Prx1* promoter (Fig. 1B). We genotyped the *NO66*$^{f/f}$, *Prx1-Cre; NO66*$^{f/+}$ and *Prx1-Cre; NO66*$^{f/f}$ mice using Southern blot (Fig. 1C) and PCR assays (Fig. 1 D and E). We performed qPCRs to examine a reduction of *NO66* expression in mouse skeleton. We observed a marked decrease in *NO66* mRNA expression in whole tissues such as limbs, calvaria, and ventral part of ribs in homozygous *Prx1-Cre; NO66*$^{f/f}$ mice at different developmental stages (Fig. 1F). To determine whether NO66 protein was completely depleted from cells of mesenchymal lineage in the homozygous *Prx1-Cre; NO66*$^{f/f}$ mice, we performed immunostaining using anti-NO66 antibody on limb and head sections of *Prx1-Cre; NO66*$^{f/f}$ and *NO66*$^{f/f}$ embryos at embryonic day 15.5 (E15.5) as well as newborn mice at postnatal day 3 (P3). We found that in limbs of E15.5 *NO66*$^{f/f}$ control embryos NO66 protein was detectable in all cells of limbs including skins, muscles and long bones (S. Fig. 1C, 1E, 1G). NO66 protein was also detectable in all cells of presumptive calvaria of E15.5 *NO66*$^{f/f}$ embryos and calvaria of P3 *NO66*$^{f/f}$ mice (S. Fig. 2C, 2G). However, in limbs of E15.5 homozygous *Prx1-Cre; NO66*$^{f/f}$ embryos, NO66 protein were no longer detectable in chondrocytes and cells in the perichondral/periosteal regions of developing long bones (S. Figs. 1D, 1F, 1H), where the *Prx1* promoter was shown to be active. [22] As a control, the NO66 protein was still present in skin, muscle and bone marrow of those *Prx1-Cre; NO66*$^{f/f}$ embryos (S. Figs. 1D, 1F, 1H), in which the *Prx1* promoter was demonstrated to be inactive. [22] Moreover, we found that NO66 protein was still detectable in some cells of presumptive calvaria of E15.5 *Prx1-Cre; NO66*$^{f/f}$ embryos (S. Fig. 2D) and endosteal cells in calvaria of P3 *Prx1-Cre; NO66*$^{f/f}$ mice (S. Fig. 2H), indicating an incomplete depletion of *NO66* in cells of developing mouse calvaria.

In addition, we performed qPCR assay on heterozygous *Prx1-Cre; NO66*$^{f/+}$ mice. We found that *NO66* expression was significantly reduced in limbs and calvaria of the heterozygous *Prx1-Cre; NO66*$^{f/+}$ mice when compared to those of *NO66*$^{f/f}$ controls (S. Fig. 3; $p < 0.05$).

Increase in Accumulation of Endochondral and Intramembranous Bones of Mesenchymal *NO66*-Knockout Mice during Skeletal Development

Adult male and female homozygous *Prx1-Cre; NO66$^{f/f}$* mice were viable and fertile. We observed that the average body weights and lengths of newborn as well as two-month-old *Prx1-Cre; NO66$^{f/f}$* mice were significantly greater than those of *NO66$^{f/f}$* mice (S. Fig. 4 and S. Fig. 5; $p < 0.05$). By comparison, we did not observe a significant difference in body weights and lengths between heterozygous *Prx1-Cre; NO66$^{f/+}$* and *NO66$^{f/f}$* mice (S. Fig. 4 and S. Fig. 5; $p > 0.05$). Skeleton preparation showed that the ossified regions in skulls and limbs of the homozygous *Prx1-Cre; NO66$^{f/f}$* embryos were larger than those of *NO66$^{f/f}$* littermates on embryonic day 18.5 (E18.5) (Fig. 2), suggesting an increase in intramembranous and endochondral bone formation.

To confirm the increase of bone formation, we performed Alcian blue and von Kossa staining of long bone and calvarial sections from mice at different developmental stages. Alcian blue staining showed that in femurs of E14.5 and E15.5 homozygous *Prx1-Cre; NO66$^{f/f}$* embryos, the hypertrophic zone (Fig. 3C) and primary ossification center (Fig. 3G) were larger than those in femurs of *NO66$^{f/f}$* controls (Fig. 3 A and E; S. Fig. 6), implicating an increase in hypertrophic chondrocyte differentiation and primary ossification. von Kossa staining revealed more mineralized tissues in periostea as well as primary ossification center of femurs of homozygous *Prx1-Cre; NO66$^{f/f}$* embryos (Fig. 3 D and H) than in those of *NO66$^{f/f}$* controls (Fig. 3 B and F), suggesting accelerated endochondral bone formation. Consistent with these observations, immunostaining of type I collagen (COL1), a marker of bone tissue, showed more COL1 in the periostea and primary ossification center of femurs of the E14.5 and E15.5 homozygous *Prx1-Cre; NO66$^{f/f}$* embryos (Fig. 3 K, L, O, and P) than in the femurs of *NO66$^{f/f}$* controls (Fig. 3 I, J, M, and N). Similarly, immunostaining of type 10 collagen (COL10), a marker of hypertrophic chondrocytes, showed more COL10 in the hypertrophic zone of femurs in those E14.5 homozygous *Prx1-Cre; NO66$^{f/f}$* embryos (S. Fig. 7B) than in the femurs of *NO66$^{f/f}$* controls (S. Fig. 7A). In addition, von Kossa and immunostaining revealed more mineralized tissues, more COL1 and BSP, another marker of bone formation, in calvaria of newborn homozygous *Prx1-Cre; NO66$^{f/f}$* mice (Fig. 3 T, W and X) than in calvaria of *NO66$^{f/f}$* controls (Fig. 3 R, U and V). By comparison, we did not observe overt differences in Alcian blue, von Kossa and COL1 staining of femurs of the E15.5 heterozygous *Prx1-Cre; NO66$^{f/+}$* embryos when compared to those of *NO66$^{f/f}$* controls (S. Fig. 8). We therefore selected the homozygous *Prx1-Cre; NO66$^{f/f}$* mice and *NO66$^{f/f}$* controls for further analyses.

A High-Bone-Mass Phenotype in Adult Mesenchymal *N066*-Knockout Mice

To determine whether the mesenchymal deletion of *NO66* continued to lead to the presence of more bones and affect bone homeostasis in adult mice, we used μCT scan to analyze the long bones and calvaria of *NO66$^{f/f}$* and *Prx1-Cre; NO66$^{f/f}$* mice at two months of age. The results revealed greater bone mineral density, percentage of bone volume, and cortical bone thickness in distal femurs of the *Prx1-Cre; NO66$^{f/f}$* mice than in those of controls (Fig. 4 A-D; $p < 0.01$). Moreover, the calvaria of the *Prx1-Cre; NO66$^{f/f}$* mice were significantly thicker than those of the controls (Fig. 4 E and F; $p < 0.01$), indicating a high-bone-mass phenotype. Von Kossa and Safranin O staining showed more mineralized tissues or

trabeculae in the distal femurs of those *Prx1-Cre; NO66*$^{f/f}$ mice than in those of the controls (Fig. 5 A-D). Furthermore, bone histomorphometry indicated that in the *Prx1-Cre; NO66*$^{f/f}$ mice, the number of osteoblasts was increased, whereas the number of osteoclasts was decreased (Fig. 5 I and J; Tables S1 and S2; S. Fig. 9), resulting in an increased bone-formation rate (Fig. 5 E-H and K; Table S1). These results suggested that ablation of *NO66* in *Prx1-Cre* expressing cells continued to affect adult bone homeostasis, leading to a high bone mass phenotype.

Increase in Number of Osx-Expressing Preosteoblasts and Osteoblasts in Endochondral and Membranous Bones of Mesenchymal *NO66*-Knockout Mice

In our previous *in vitro* cell culture study, we showed that *NO66* knockdown in MC3T3 preosteoblasts accelerated osteoblast differentiation. [20] Because the adult *Prx1-Cre; NO66*$^{f/f}$ mice had increased numbers of osteoblasts, we wanted to know whether it was due to an increase in the number of preosteoblasts, or an increase in the differentiation of preosteoblasts into mature osteoblasts. During early skeletal development in mouse embryos, generation of osteoprogenitors or preosteoblasts first occurs in the perichondrium and periosteum in long bones and presumptive calvaria on about E13. Since *Osx* is highly expressed in cells of osteoblast-lineage, we performed immunostaining of Osx to mark the preosteoblasts and osteoblasts in periosteal regions of mouse long bones and calvaria. The staining results demonstrated that the numbers of Osx-positive cells in periosteal regions of femurs in *Prx1-Cre; NO66*$^{f/f}$ embryos were significantly higher than those in these regions in their *NO66*$^{f/f}$ littermates at E14.5, E15.5, and E18.5 (Fig. 6 A-L; Table 1; $p < 0.01$), suggesting an increase in the number of preosteoblasts and/or osteoblasts. We observed similar results in calvaria of newborn *Prx1-Cre; NO66*$^{f/f}$ and *NO66*$^{f/f}$ mice (Fig. 6 M-P; Table 1).

Preosteoblasts are proliferating cells and predominantly locate in the periosteal regions of long bones and calvaria. To determine whether the number of proliferating cells were increased in the periosteal regions of long bones and calvaria of E15.5 *Prx1-Cre; NO66*$^{f/f}$ embryos, we performed BrdU incorporation. We found more BrdU-positive cells in the perichondrium and periosteum in femurs of E15.5 *Prx1-Cre; NO66*$^{f/f}$ embryos than in *NO66*$^{f/f}$ controls (Fig. 7 A, B and E; $p < 0.05$). We observed similar results in the presumptive calvaria of those *Prx1-Cre; NO66*$^{f/f}$ and *NO66*$^{f/f}$ embryos (Fig. 7 C-E; $p < 0.05$). These results indicated that deletion of *NO66* in *Prx1-Cre* expressing mesenchymal cells increased the number of proliferating cells in the periosteal region and in calvaria. This increase is also consistent with the observed increase in the number of preosteoblasts.

Increase in Expression of Genes in Embryonic Limbs and Adult Calvaria of Mesenchymal *NO66*-Knockout Mice

Formation of normal bones depends upon a balance between osteoblast-involved bone formation and osteoclast-mediated bone resorption. The generation and function of osteoblasts are regulated by diverse signals, including BMP, IGF and Wnt signaling pathways. [25] At the same time, osteoblasts produce osteoprotegerin (Opg); a decoy inhibitor of receptor activator of nuclear factor-κB ligand (Rankl), which itself is an activator of osteoclastogenesis and in bone resorption. [26] To determine whether an

acceleration of primary ossification in the limbs of *NO66* mutant embryos could be associated with changes in expression of marker genes and their upstream signaling molecules, we performed qPCRs using total RNA obtained from limbs of E13.5 *NO66*$^{f/f}$ and *Prx1-Cre; NO66*$^{f/f}$ embryos (Fig. 7 F). We found that expression of *Bmp2*, *Bmpr1b*, and *Igf1* mRNA was upregulated concurrently with elevated expression of osteoblast and hypertrophic chondrocyte differentiation markers, such as *Runx2*, *Osx*, *ALP*, *Col1 (Col1a1)*, and *Col10*, in limbs of E13.5 *Prx1-Cre; NO66*$^{f/f}$ embryos when compared to those in their controls. By comparison, expression of *Tcf*, a downstream effector of Wnt signaling, and *Ihh* was not significantly changed (Fig. 7 F; $p > 0.05$).

To further confirm whether expression of the above genes was increased in osteoblast-lineage-enriched calvaria of the adult *NO66* mutant mice, we performed qPCRs using total RNA obtained from calvaria of one-month-old *NO66*$^{f/f}$ and *Prx1-Cre; NO66*$^{f/f}$ mice (Fig. 7 G). We again observed an upregulaton of expression of *Bmp2*, *Igf1* and *Osx*, but not *Bmpr1b*, *Igf1r* and *Runx2* (Fig. 7 G; $p > 0.05$); this upregulation was accompanied by an increase in the expression of bone formation markers, including *ALP*, *Cola1* and *Bsp*, in calvaria of the *Prx1-Cre; NO66*$^{f/f}$ mice (Fig. 7 G; $p < 0.05$). Moreover, expression of *Opg* was markedly increased (Fig. 7 G; $p < 0.01$), whereas expression of *Rankl* did not change significantly in calvaria of these *Prx1-Cre; NO66*$^{f/f}$ mice (Fig. 7 G; $p > 0.05$). By comparison, expression of *TRAP* (Tartrate-resistant acid phosphatase), a marker of osteoclast activity, was downregulated in calvaria of the *Prx1-Cre; NO66*$^{f/f}$ mice (Fig. 7 G; $p < 0.05$). These results suggested that NO66 might negatively regulate expression of *Bmp2*, *Igf1* and *Opg* to control bone formation and bone resorption.

Increase in Levels of H3K4me3 and H3K36me3 in Long Bones of Mesenchymal *NO66*-Knockout Mice

We previously showed that NO66 has histone demethylase activity for H3K4me3 and H3K36me3. [20] To determine whether mesenchymal deletion of *NO66* altered cellular levels of these chromatin marks, we performed immunostaining using an antibody against H3K4me3 or H3K36me3 on femur sections obtained from *NO66*$^{f/f}$ and *Prx1-Cre; NO66*$^{f/f}$ mouse embryos at E15.5 and E18.5. We observed increased staining of H3K4me3 and H3K36me3 in proliferating and prehypertrophic chondrocytes as well as cells in perichondral/periosteal regions of femurs from E15.5 or E18.5 *Prx1-Cre; NO66*$^{f/f}$ embryos, when compared to those from *NO66*$^{f/f}$ controls (S. Fig. 10). To further confirm this observation, we performed Western blots to measure levels of H3K4me3 and H3K36me3 in femurs of E18.5 *NO66*$^{f/f}$ and *Prx1-Cre; NO66*$^{f/f}$ embryos. We observed the increased levels of H3K4me3 and H3K36me3 in femurs of E18.5 *Prx1-Cre; NO66*$^{f/f}$ embryos (S. Fig. 11), consistent with the immunostaining results.

Discussion

In this study, we used a genetically engineered mouse model to study the *in vivo* function of NO66 in bone formation. Our results showed first that deletion of *NO66* in *Prx1-Cre*-expressing mesenchymal cells leads to an increase in endochondral bone development. This included earlier hypertrophic chondrocyte differentiation and subsequent bone formation,

suggesting that the entire process of endochondral bone development might be accelerated. At E18.5, membranous bone ossification was also markedly increased which could be consistent with the hypothesis that this process too was accelerated. The increased number of preosteoblasts and osteoblasts in the *NO66* mutant embryos at defined time points could be a consequence of the acceleration of endochondral bone development. We hypothesize that the persistence of increased numbers of osteoblast lineage cells in adult animals leads to a high-bone-mass phenotype. In the *NO66* mutant embryos, there was also a higher level expression of several genes, including *Bmp2*, *Igf1*, *Osx* and *Opg*. These *in vivo* observations suggested that NO66 plays an important physiological role in bone formation probably by controlling the timing of bone development as well as the number of osteoblast lineage cells, and also by regulating the expression of a number of genes that are critical for these processes.

Our previous *in vitro* study reported that knockdown of *NO66* in MC3T3 preosteoblasts increased osteoblast mineralization, suggesting a negative regulator of NO66 in preosteoblast differentiation. [20] What distinguishes the present *in vivo* findings from these *in vitro* results is that *in vivo* the developmental process of endochondral bone formation and maybe that of the membranous skeleton are accelerated, and as a possible result of this acceleration, the number of Osx-positive cells is increased. We therefore postulate that NO66 not only regulates preosteoblast differentiation but also plays an important role in the *in vivo* commitment or differentiation of osteochondroprogenitors. [6] We also hypothesize that in *Prx1-Cre; NO66$^{f/f}$* embryos, the increase in the number of Osx-expressing cells, which represent preosteoblasts and osteoblasts in the periostea and calvaria, is likely responsible for the increased bone formation in these embryos. Moreover, the increased number of osteoblasts measured by histomorphometry in adult *Prx1-Cre; NO66$^{f/f}$* mice was also consistent with the increased numbers of Osx-positive cells in bones during embryonic development. However, we note that *ex vivo* cultured osteoblasts from *NO66$^{f/f}$* and *Prx1-Cre; NO66$^{f/f}$* mice did not reveal significant differences in differentiation of the cells (data not shown), which was attributed to a mixed population of cells due to incomplete deletions of *NO66*. Therefore, whether or not the effects of NO66 observed in the *Prx1-Cre; NO66$^{f/f}$* mice are cell-autonomous remains to be determined.

Although we do not yet know which specific molecular mechanisms control the acceleration of endochondral bone development as well as the increased number of preosteoblasts/osteoblasts in bones of *Prx1-Cre; NO66$^{f/f}$* embryos and adult mice, several signaling molecules may have a role in these controls. We measured the mRNA expression for only a limited number of genes in limbs and calvaria of *NO66$^{f/f}$* and *Prx1-Cre; NO66$^{f/f}$* mice in this study, and observed a consistent increase in *Bmp2*, *Igf1* and *Osx* mRNA expression in the *Prx1-Cre; NO66$^{f/f}$* mice. Because BMP2 and IGF1 are important signaling molecules that can induce expression of *Osx*,[7, 8, 27] we speculate that upregulation of *Bmp2* and *Igf1* expression in bones of the *Prx1-Cre; NO66$^{f/f}$* mice may contribute, at least in part, to the elevated expression of *Osx* and an increase in the number of Osx-expressing preosteoblasts/osteoblasts. Nevertheless, other signaling molecules may have similar roles in the regulation of *Osx* expression and the number of Osx-expressing cells. We previously found that expression of *Osx* mRNA was not affected by shRNA knockdown of *NO66* in MC3T3

preosteoblasts. [20] This led us to hypothesize that the *in vivo* increased expression of *Bmp2* and *Igf1* might be responsible for the concurrent elevation in *Osx* expression in the *NO66* mutant mice. The increase in *Osx* mRNA should also amplify the effects of the larger number of Osx-expressing cells in bone formation. Whether NO66 directly regulates expression of *Bmp2* and *Igf1* remains to be defined.

It has been known that the osteoblasts produce both OPG and Rankl. [26] Since expression of *Opg*, but not *Rankl* mRNA, was increased in calvaria of the *Prx1-Cre; NO66*$^{f/f}$ mice, it implied that NO66 negatively regulates expression of *Opg* gene. Moreover, because OPG is an inhibitor of osteoclastogenesis, [26] the finding that *Opg* mRNA was increased in *NO66* mutant calvaria, but not that of *Rankl*, may explain the decreased osteoclast numbers in those mice. The lower osteoclast numbers likely contributed to the increased bone mass in *Prx1-Cre; NO66*$^{f/f}$ mice. Given that *Opg* expression is not directly regulated by Osx, [28] upregulation of *Opg* mRNA expression observed in calvaria of the *Prx1-Cre; NO66*$^{f/f}$ mice is less likely secondary to the increased Osx activity. Because TRAP is an important marker of osteoclasts, we speculate that the lower number of osteoclasts is likely responsible for the moderate decrease in *TRAP* mRNA expression in bones of the *Prx1-Cre; NO66*$^{f/f}$ mice.

We previously reported that NO66 has histone demethylase activity for H3K4me3 and H3K36me3. [20] The increased levels of H3K4me3 and H3K36me3 in bones of the *Prx1-Cre; NO66*$^{f/f}$ embryos are consistent with this previous report. Since H3K4me3 and H3K36me3 are regarded as two marks of transcriptionally active chromatin, it is likely that NO66 controls expression of genes, such as *Bmp2*, *Igf1* and/or *Opg*, via a change in histone methylation state in the chromatin of these genes. However, at the moment we do not yet know whether the increased levels of H3K4me3 and H3K36me3 in the *Prx1-Cre; NO66*$^{f/f}$ embryos were solely or directly caused by depletion of *NO66*. Given that the methylation state of histone H3 at lysine 4 and lysine 36 can be affected by many other histone demethylases, it is possible that deletion of *NO66* interferes with the activity of other histone demethylase(s) which may then contribute to the increased levels of H3K4me3 and H3K36me3 in those embryos. Nevertheless, whether NO66 affects other histone demethylase(s) and whether *NO66*-deletion-mediated increases in H3K4me3 and H3K36me3 are cell-autonomous still remain to be determined.

Taken together, our data provide evidence that NO66 plays an important role in osteogenesis during mouse development as well as bone homeostasis in adult mice. NO66 controls osteogenesis by regulating the process of endochondral and membranous skeletal development, by controlling the number of preosteoblasts/osteoblasts, and the expression of a number of genes which are important for bone formation. Identification of the NO66 downstream targets will be a main focus in a future study.

Supplementary Material

Refer to Web version on PubMed Central for supplementary material.

Acknowledgments

We thank Zhaoping Zhang for mES microinjection, and Michael Starbuck for histomorphometric analyses. We also thank Donald R. Norwood for editing our manuscript. This study was supported by National Institutes of Health grant R01 AR49072 (to B.d.C.), the MD Anderson Cancer Center Support Grant CA016672, the 2012 Rolanette and Berdon Lawrence Bone Research Award (to Q.C.), the Children Sarcoma Initiative and the Triumph Over Kid Cancer Foundation (to Q.C.), the Ben F. Love Endowment (to R.R.B.).

Authors' Role: Study design: QC and BdC. Study conduct: QC, KS and JMD. Data interpretation: QC and BdC. Contributed reagents/materials/suggestions/analysis tools: HY, RK and RRB. Manuscript preparation: QC and BdC.

References

1. Ducy P, Zhang R, Geoffroy V, Ridall AL, Karsenty G. Osf2/Cbfa1: a transcriptional activator of osteoblast differentiation. Cell. 1997; 89(5):747–54. [PubMed: 9182762]
2. Komori T, Yagi H, Nomura S, Yamaguchi A, Sasaki K, Deguchi K, et al. Targeted disruption of Cbfa1 results in a complete lack of bone formation owing to maturational arrest of osteoblasts. Cell. 1997; 89(5):755–64. [PubMed: 9182763]
3. Otto F, Thornell AP, Crompton T, Denzel A, Gilmour KC, Rosewell IR, et al. Cbfa1, a candidate gene for cleidocranial dysplasia syndrome, is essential for osteoblast differentiation and bone development. Cell. 1997; 89(5):765–71. [PubMed: 9182764]
4. Nakashima K, Zhou X, Kunkel G, Zhang Z, Deng JM, Behringer RR, et al. The novel zinc finger-containing transcription factor osterix is required for osteoblast differentiation and bone formation. Cell. 2002; 108(1):17–29. [PubMed: 11792318]
5. Zhou X, Zhang Z, Feng JQ, Dusevich VM, Sinha K, Zhang H, et al. Multiple functions of Osterix are required for bone growth and homeostasis in postnatal mice. Proc Natl Acad Sci U S A. 2010; 107(29):12919–24. [PubMed: 20615976]
6. Nakashima K, de Crombrugghe B. Transcriptional mechanisms in osteoblast differentiation and bone formation. Trends Genet. 2003; 19(8):458–66. [PubMed: 12902164]
7. Celil AB, Hollinger JO, Campbell PG. Osx transcriptional regulation is mediated by additional pathways to BMP2/Smad signaling. J Cell Biochem. 2005; 95(3):518–28. [PubMed: 15786511]
8. Celil AB, Campbell PG. BMP-2 and insulin-like growth factor-I mediate Osterix (Osx) expression in human mesenchymal stem cells via the MAPK and protein kinase D signaling pathways. J Biol Chem. 2005; 280(36):31353–9. [PubMed: 16000303]
9. Monroe DG, McGee-Lawrence ME, Oursler MJ, Westendorf JJ. Update on Wnt signaling in bone cell biology and bone disease. Gene. 2012; 492(1):1–18. [PubMed: 22079544]
10. Hu H, Hilton MJ, Tu X, Yu K, Ornitz DM, Long F. Sequential roles of Hedgehog and Wnt signaling in osteoblast development. Development. 2005; 132(1):49–60. [PubMed: 15576404]
11. Day TF, Yang Y. Wnt and hedgehog signaling pathways in bone development. J Bone Joint Surg Am. 2008; 90 Suppl 1:19–24. [PubMed: 18292352]
12. Martin C, Zhang Y. The diverse functions of histone lysine methylation. Nat Rev Mol Cell Biol. 2005; 6(11):838–49. [PubMed: 16261189]
13. Lachner M, Jenuwein T. The many faces of histone lysine methylation. Curr Opin Cell Biol. 2002; 14(3):286–98. [PubMed: 12067650]
14. Klose RJ, Kallin EM, Zhang Y. JmjC-domain-containing proteins and histone demethylation. Nat Rev Genet. 2006; 7(9):715–27. [PubMed: 16983801]
15. Shi Y, Whetstine JR. Dynamic regulation of histone lysine methylation by demethylases. Mol Cell. 2007; 25(1):1–14. [PubMed: 17218267]
16. Eilbracht J, Reichenzeller M, Hergt M, Schnolzer M, Heid H, Stohr M, et al. NO66, a highly conserved dual location protein in the nucleolus and in a special type of synchronously replicating chromatin. Mol Biol Cell. 2004; 15(4):1816–32. [PubMed: 14742713]
17. Suzuki C, Takahashi K, Hayama S, Ishikawa N, Kato T, Ito T, et al. Identification of Myc-associated protein with JmjC domain as a novel therapeutic target oncogene for lung cancer. Mol Cancer Ther. 2007; 6(2):542–51. [PubMed: 17308053]

18. Kirienko NV, Fay DS. SLR-2 and JMJC-1 regulate an evolutionarily conserved stress-response network. EMBO J. 2010; 29(4):727–39. [PubMed: 20057358]
19. Rogers R, Dharsee M, Ackloo S, Flanagan JG. Proteomics analyses of activated human optic nerve head lamina cribrosa cells following biomechanical strain. Invest Ophthalmol Vis Sci. 2012; 53(7):3806–16. [PubMed: 22589438]
20. Sinha KM, Yasuda H, Coombes MM, Dent SY, de Crombrugghe B. Regulation of the osteoblast-specific transcription factor Osterix by NO66, a Jumonji family histone demethylase. EMBO J. 2010; 29(1):68–79. [PubMed: 19927124]
21. Brien GL, Gambero G, O'Connell DJ, Jerman E, Turner SA, Egan CM, et al. Polycomb PHF19 binds H3K36me3 and recruits PRC2 and demethylase NO66 to embryonic stem cell genes during differentiation. Nat Struct Mol Biol. 2012; 19(12):1273–81. [PubMed: 23160351]
22. Logan M, Martin JF, Nagy A, Lobe C, Olson EN, Tabin CJ. Expression of Cre Recombinase in the developing mouse limb bud driven by a Prxl enhancer. Genesis. 2002; 33(2):77–80. [PubMed: 12112875]
23. Chen Q, Liu W, Sinha KM, Yasuda H, de Crombrugghe B. Identification and characterization of microRNAs controlled by the osteoblast-specific transcription factor Osterix. PLoS One. 2013; 8(3):e58104. [PubMed: 23472141]
24. Chen Q, Liang D, Fromm LD, Overbeek PA. Inhibition of lens fiber cell morphogenesis by expression of a mutant SV40 large T antigen that binds CREB-binding protein/p300 but not pRb. J Biol Chem. 2004; 279(17):17667–73. [PubMed: 14742445]
25. Canalis E. Growth factor control of bone mass. J Cell Biochem. 2009; 108(4):769–77. [PubMed: 19718659]
26. Kobayashi Y, Udagawa N, Takahashi N. Action of RANKL and OPG for osteoclastogenesis. Crit Rev Eukaryot Gene Expr. 2009; 19(1):61–72. [PubMed: 19191757]
27. Zhang W, Shen X, Wan C, Zhao Q, Zhang L, Zhou Q, et al. Effects of insulin and insulin-like growth factor 1 on osteoblast proliferation and differentiation: differential signalling via Akt and ERK. Cell Biochem Funct. 2012; 30(4):297–302. [PubMed: 22249904]
28. Cao Y, Jia SF, Chakravarty G, de Crombrugghe B, Kleinerman ES. The osterix transcription factor down-regulates interleukin-1 alpha expression in mouse osteosarcoma cells. Molecular cancer research : MCR. 2008; 6(1):119–26. [PubMed: 18234967]

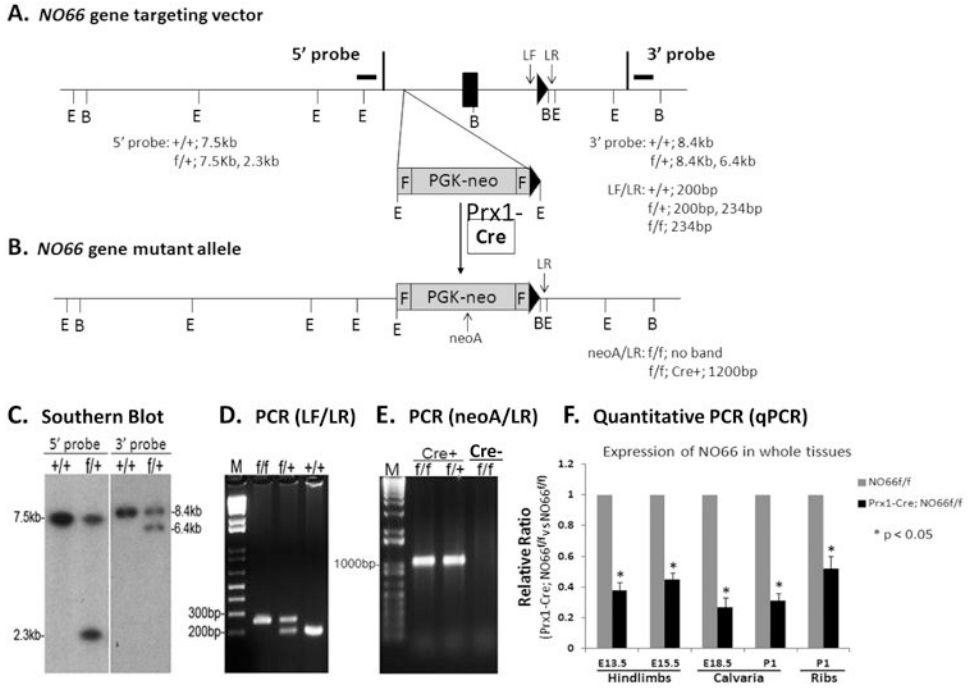

Fig. 1. Generation of mesenchyme-specific *NO66*-knockout mice

A: *NO66*-targeting vector. **B**: *NO66* mutant allele. **C**: Southern blot. The genomic DNA of mES cells or mice was digested with 5′ EcoR I (E) or 3′ BamH I (B), and blotted with indicated probes. **D** and **E**: PCR. PCR was performed using mouse tail DNA and two pairs of primers as indicated. **F**: QPCR. qPCR was performed using total RNAs from limbs, calvaria and ventral ribs of mice at different developmental stages (n = 3).

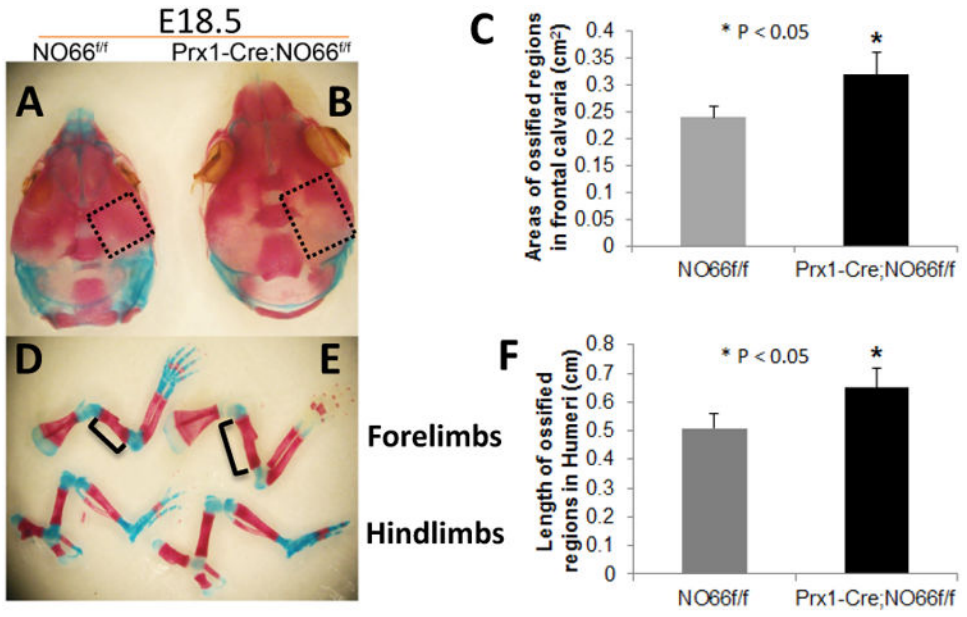

Fig. 2. Skeleton preparation

A, B, D, E: Skeleton preparation of mouse embryos at E18.5. Squares with dashed lines in A and B show the size of ossified areas in frontal calvaria; brackets in D and E indicate the length of ossified regions in humeri. **C**: Quantification of the size of ossified areas in frontal calvaria shown in A and B (n = 4). **F**: Quantification of the length of ossified regions in humeri shown in D and E (n = 8).

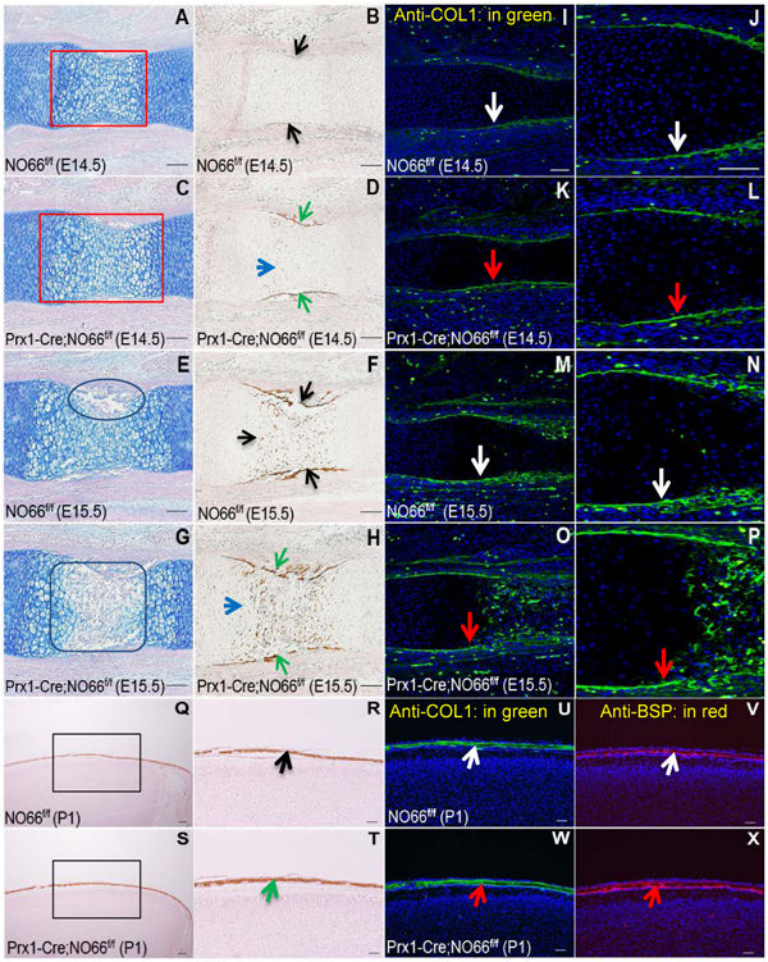

Fig. 3. Examination of bone formation in mesenchymal *NO66*-knockout mice during skeletal development

A-P: Alcian blue (A, C, E, G), von Kossa (B, D, F, H) and type I collagen (COL1) staining (green, COL1; blue, DAPI) (I-P) of femoral sections of E14.5 and E15.5 *NO66*$^{f/f}$ and *Prx1-Cre; NO66*$^{f/f}$ embryos. The red squares in A and C show hypertrophic zones; the oval in E and rounded square in G show primary ossification centers; the arrows in B, D, F, and H indicate mineralized tissues; and the arrows in I-P indicate COL1 in periostea. The images in J, L, N, and P are higher magnification of the images in I, K, M, and O, respectively. **Q-X**: von Kossa (Q-T), COL1 (U and W) and BSP (V and X) antibody staining of frontal calvaria of P1 *NO66*$^{f/f}$ and *Prx1-Cre; NO66*$^{f/f}$ mice. The staining signals are indicated by arrows. Q and S are sagittal sections of mouse heads in frontal area. R and T are higher magnification of the boxed regions in Q and S. R, U, V and T, W, X are serial sections from the same tissue block, respectively.

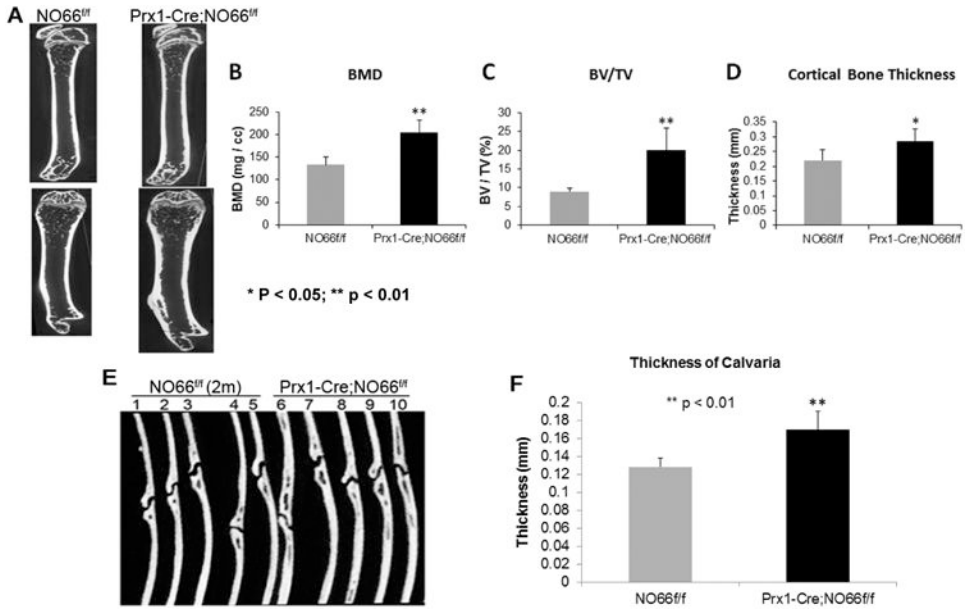

Fig. 4. Micro-computed tomography (μCT)

A: μCT images of femurs in male mice at 2 months of age (2m). **B-D**: Quantification of the μCT images shown in A. The bone mineral density (BMD), percentage of bone volume (BV) versus total volume (TV) and thickness of cortical bones are shown. **E**: μCT images of the frontal calvaria of 2m mice. **F**: Quantification of the μCT images shown in E. (n = 5)

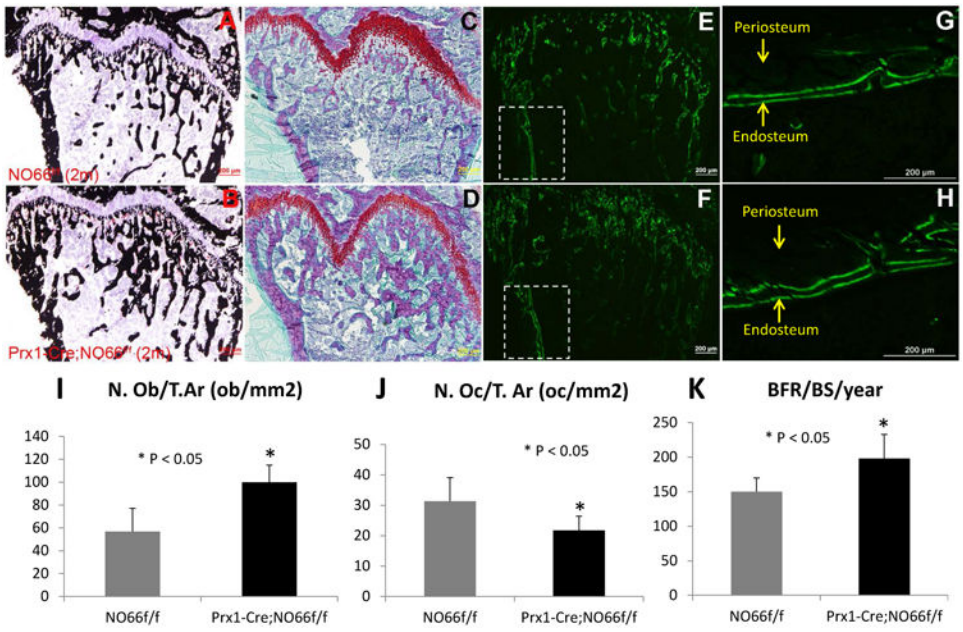

Fig. 5. Bone histological and histomorphometry in adult mesenchymal *NO66*-knockout mice

A-D: von Kossa (A and B) and Safranin O (C and D) staining of distal femur sections of 2m male *NO66*$^{f/f}$ and *Prx1-Cre; NO66*$^{f/f}$ mice. **E-H**: Double fluorochrome calcein lines in femurs of 2m *NO66*$^{f/f}$ and *Prx1-Cre; NO66*$^{f/f}$ mice. **I-K**: Histomorphometry. (**I**) Number of osteoblasts (N.Ob) per total area (T.Ar) analyzed; (**J**) Number of osteoclasts (N.Oc) per total area (T.Ar) analyzed; (**K**) Bone formation rate (BFR) per bone surface (BS) analyzed per year. (n = 4)

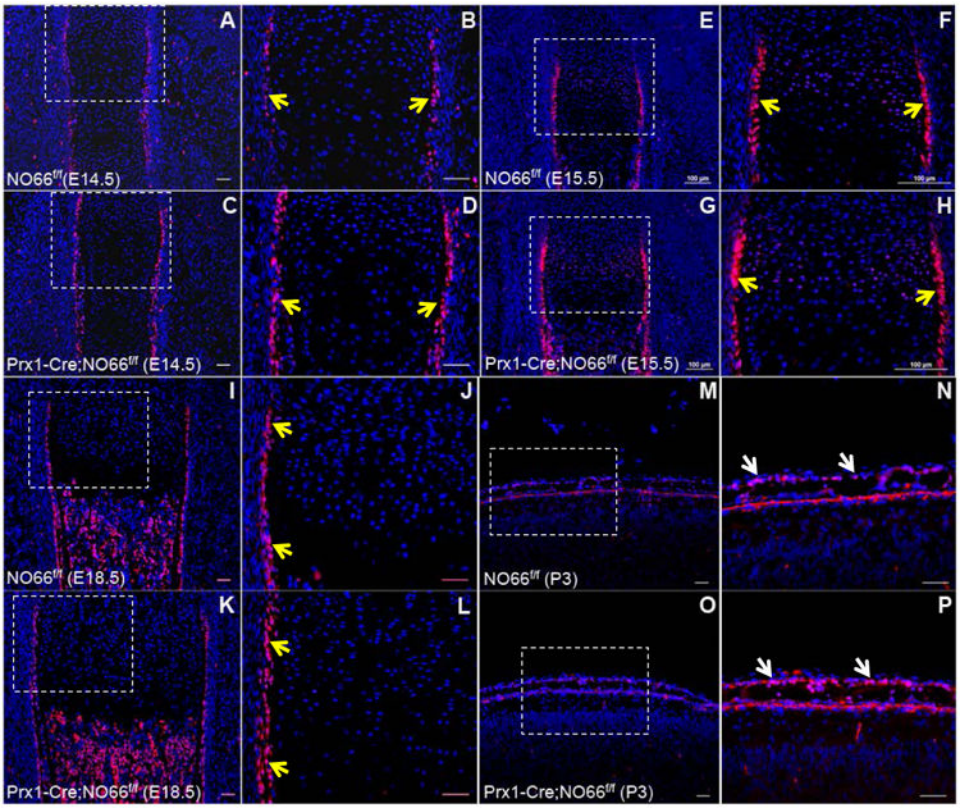

Fig. 6. Immunostaining for Osx

A-L: Femur sections of *NO66$^{f/f}$* (A, B, E, F, I, J) and *Prx1-Cre; NO66$^{f/f}$* (C, D, G, H, K, L) embryos on E14.5, E15.5, and E18.5. **M-P**: Frontal calvarial sections of *NO66$^{f/f}$* (M, N) and *Prx1-Cre; NO66$^{f/f}$* (O, P) mice at postnatal day 3 (P3). B, D, F, H, J, L, N and P are higher magnification images of the boxed areas in A, C, E, G, I, K, M and O, respectively. The yellow and white arrows indicate Osx-positive cells in periosteal regions of femurs and calvaria. (Red, Osx; Blue, DAPI)

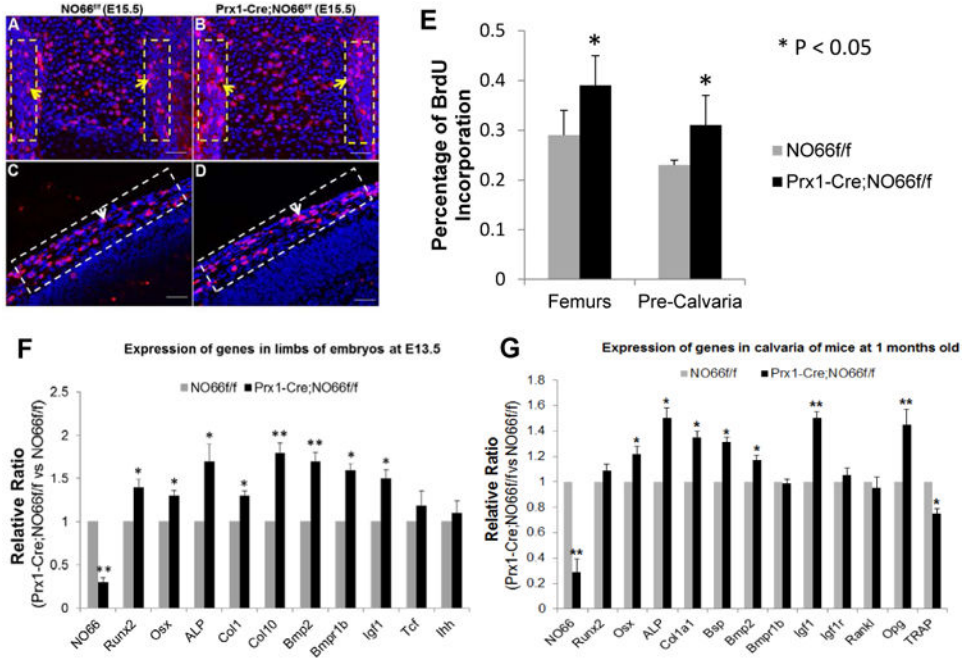

Fig. 7. BrdU Incorporation and qPCR Assays

A-D: BrdU Incorporation. The femur (A, B) and head (C, D) sections of E15.5 *NO66$^{f/f}$* and *Prx1-Cre; NO66$^{f/f}$* embryos were stained using anti-BrdU antibody (red, BrdU; blue, DAPI). The yellow and white arrows indicate the BrdU-positive cells in the boxed periosteal areas of femurs and presumptive frontal calvaria. **E**: Percentage of BrdU-positive cells in the boxed areas shown in A-D. **F**: Results of qPCRs using total RNAs from limbs of E13.5 *NO66$^{f/f}$* and *Prx1-Cre; NO66$^{f/f}$* embryos (* $p < 0.05$; ** $p < 0.01$; $n = 3$). **G**: Results of qPCRs using total RNAs from calvaria of 1m male *NO66$^{f/f}$* and *Prx1-Cre; NO66$^{f/f}$* mice (* $p < 0.05$; ** $p < 0.01$; $n = 3$).

Table 1
Percentage of Osx-Positive Cells per Area Analyzed

	Mean percentage ± S.D.			
Mice	**E14.5**	**E15.5**	**E18.5**	**P3 (calvaria)**
$NO66^{f/f}$	18.0 ± 2.5	30.1 ± 2.7	40.5 ± 3.1	12.9 ± 1.9
Prx1-Cre; $NO66^{f/f}$	38.3 ± 4.5*	48.9 ± 3.9*	60.6 ± 4.1*	21.8 ± 2.6*

* $p < 0.01$; n = 3